

# Nonintrusive Uncertainty Quantification in the Simulation of Steel Reheating Using Polynomial Chaos Expansion

Marks Legkovskis,\* Peter J. Thomas, and Michael Auinger

Uncertainty quantification (UQ) is deemed critical in steel reheating simulations due to the significant input uncertainties arising when defining steel surface properties and atmospheric furnace conditions. In order to conduct UQ, the study utilizes polynomial chaos expansion, which has been found to significantly curtail the computational effort needed to obtain reliable convergent statistics for the model of interest. Results from a comprehensive UQ analysis of a walking-beam reheat furnace simulated using Tata Steel's reheat furnace control model, online slab temperature calculation, are presented. Slab temperature evolution and oxide scale growth are chosen as the study's QoIs. The analysis reveals that at the earlier stages of reheating, the majority of the output variance in slab temperature can be traced back exclusively to the emissivity of the slab surface, and the majority of the output variance in oxide scale growth is traced back to the combination of slab's surface emissivity and the initial scale thickness found on steel products prior to reheating. However, as the steel product advances toward the furnace's discharge end, inputs related to oxide scale growth become increasingly important, ultimately becoming the most influential input parameters, although the dynamics of this transition differ between the QoIs.

significant progress has been made in modeling furnace operations for steel reheating both via mathematical<sup>[1,2]</sup> and physical approaches based on computational fluid dynamics (CFD).<sup>[3–5]</sup>

Nonetheless, the numerical modeling of the steel reheating process still involves significant challenges. These often stem from the inevitable growth of the oxide scale dictating the emissivity of the slab surface,<sup>[6]</sup> which, in turn, affects (slows down) the heat transfer to the steel. Moreover, the emissivity of the steel surface depends not only on the thickness of the oxide scale but also on its topology (i.e., porosity), the composition of the in-furnace gas atmosphere, steel grade, temperature, and how long the product spends inside the furnace (referred to as residence time). These parameter interactions are very complex to model, vary with temperature,<sup>[7]</sup> and therefore, are often neglected.<sup>[8]</sup> This parameter space comes on top of the already complex, nonlinear heat transfer models used to

## 1. Introduction

Steel reheating is an integral part of the steelmaking process responsible for raising the temperature of the semifinished steel products such as billets, blooms, or slabs to the uniform optimum temperature ( $\approx 1250^\circ\text{C}$ ) until they are plastic enough to be rolled to the desired specification. Due to the need to reduce vast energy usage and substantial product loss as oxide scale,


simulate a reheating process, where the heat transfer performances are highly sensitive to the furnace operating conditions. Therefore, rigorous model validation against experimental data, such as an instrumental slab trial,<sup>[9]</sup> is critical to the development of reheat furnace models. Moreover, in scenarios where models are associated with uncertainty, the validation process needs to be enhanced. This is often done using uncertainty quantification (UQ) techniques.<sup>[10]</sup> UQ seeks to characterize all significant uncertainties in a simulation and to quantify their effects on computed quantity(s) of interest (QoI).

The various reheat furnace models involved require input parameters such as slab and oxide scale properties as well as atmospheric furnace conditions at elevated temperatures, which are often uncertain as they are challenging, expensive to measure in accompanying experiments.<sup>[11]</sup> In such scenarios, UQ is crucial for model robustness and credibility as it allows to predict whether a process will operate in the design range when subject to uncertainties, facilitating risk-informed decision-making.

In modeling, uncertainty arises when one has imperfect information about a given parameter, which is characterized by a probability density function (PDF) as part of UQ approach. Therefore, to propagate uncertainty through a simulation model, UQ analysis involves transitioning from singular, deterministic computations to sampling-based probabilistic approaches such as Monte Carlo (MC) sampling technique. However, due to the relatively high computational costs of reheat furnace

M. Legkovskis, M. Auinger  
Advanced Manufacturing & Materials Centre  
WMG University of Warwick  
Coventry CV4 7AL, UK  
E-mail: Marks.Legkovskis@warwick.ac.uk

P. J. Thomas  
Fluid Dynamics Research Centre  
School of Engineering  
University of Warwick  
Coventry CV4 7AL, UK

 The ORCID identification number(s) for the author(s) of this article can be found under <https://doi.org/10.1002/srin.202200538>.

© 2023 The Authors. Steel Research International published by Wiley-VCH GmbH. This is an open access article under the terms of the Creative Commons Attribution License, which permits use, distribution and reproduction in any medium, provided the original work is properly cited.

DOI: 10.1002/srin.202200538

simulations, the direct use of MC in probabilistic UQ is prohibitive. A way to overcome such scenarios is to build a surrogate model capable of mimicking the input/output behavior of the underlying simulation model as closely as possible while being computationally cheap(er) to evaluate.<sup>[12]</sup> Polynomial chaos expansion (PCE)<sup>[13]</sup> is a nonintrusive (i.e., treats the underlying simulation model as a black box problem) surrogate modeling technique from the class of stochastic expansion methods that employs polynomials that are orthogonal with respect to the PDF of the uncertain input variables and is compatible with efficient sampling techniques allowing to build surrogates based on a relatively small number of samples.

PCE has drawn increasing attention due to its ability to provide exponential convergence of QoI's moments (i.e., mean or variance) at low computational costs in smooth models<sup>[14]</sup> with finite variance.<sup>[15]</sup> Since the reheat furnace models are generally smooth, at least when it comes to the prediction of slab temperature, and due to the PCE's widespread adoption for UQ purposes,<sup>[10,16,17]</sup> PCE will be used as the surrogate model technique in this study.

At present, UQ via PCE has been successfully applied in the areas of stability and control,<sup>[18]</sup> solid mechanics,<sup>[19]</sup> electronic circuits,<sup>[20]</sup> and computational fluid dynamics<sup>[21]</sup> but not in the field of steel reheating models. However, as discussed above, the reheat furnace simulations are complex systems in which it is highly desirable to characterize the uncertainties and quantify their impact on the computed QoI.

Therefore, we present a case study for the PCE-based quantification of uncertainties related to the slab surface properties and furnace atmospheric conditions in an industrially implemented numerical model for slab reheating. The study's QoIs were selected to be the slab temperature evolution and the corresponding oxide scale growth.

## 2. Computational Platform

The computational platform used in this study is the in-house developed "on-line slab temperature calculation" (OLSTC) model used to simulate the reheat furnace operations at Tata Steel plants across Europe. In the following sections, we summarize the main principles of the OLSTC model and, specifically, how it calculates the slab's temperature evolution and the oxide scale growth. For more detailed information on the OLSTC model, refer to other studies.<sup>[22–24]</sup>

### 2.1. Calculation of Slab Temperature

The starting point in the slab temperature prediction is determining the heat transfer to the slab due to the incident radiation, which is the dominant mode of heat transfer in reheat furnaces.<sup>[25]</sup> For this, the furnace temperature (aka the radiation temperature),  $T_f$ , that a slab "sees" in a given zone needs to be known.  $T_f$  is estimated from the actual furnace temperatures measured by the installed thermocouples over the entire furnace length. Note that  $T_f$  does not equal a direct thermocouple reading as the measured temperature is offset by a constant temperature value based on the data from historical instrumented slab trials. With the knowledge of  $T_f$ , the heat transfer to the slab can be calculated using a formulation based on the Stefan–Boltzmann's

law,<sup>[26]</sup> which expresses the average heat transfer rate per unit area as per Equation (1)

$$q = \epsilon_{\text{slab}} \cdot \sigma \cdot (T_f^4 - T_s^4) \quad (1)$$

where  $q$  is the heat transfer rate to the slab per unit area ( $\text{Wm}^{-2}$ ),  $\sigma$  is the Stefan–Boltzmann constant ( $\text{Wm}^{-2} \text{K}^{-4}$ ),  $\epsilon_{\text{slab}}$  is the emissivity of a slab, and  $T_s$  is the slab surface temperature (K). Note, for the first calculation instance,  $T_s$  is known as it is taken as the slab charging temperature, and with the  $T_f$  predetermined,  $q$  can be calculated. With  $q$  calculated and with the temperature-dependent material (steel) properties available, the increase in the heat content of the slab is calculated using the Fourier's law of heat conduction,<sup>[27]</sup> as per Equation (2)

$$\frac{\partial^2 T_i}{\partial x^2} + \frac{q}{k} = \frac{\rho C_p}{k} \frac{\partial T_i}{\partial t} \quad (2)$$

where  $k$  ( $\text{W} \cdot \text{m}^{-1} \cdot \text{K}^{-1}$ ),  $\rho$  ( $\text{kg} \cdot \text{m}^{-3}$ ), and  $C_p$  ( $\text{J} \cdot \text{kg}^{-1} \cdot \text{K}^{-1}$ ) are the material's temperature-dependent thermal conductivity, density, and the specific heat capacity, respectively. Then, the slab's geometry is divided into several computational cells across its thickness to calculate the average temperature of the slab. For each cell,  $T_i$  is calculated using Equation (2), which allows calculating the average temperature of the slab,  $T_{\text{slab}}$ . In the next timestep and with a slab in a new position, two factors are known,  $T_f$  as it is predetermined and  $T_s$  as it can be deduced based on the cells' temperatures from the previous timestep and the assumption that there is no heat loss from within the steel slab. Thus,  $q$  and the subsequent heat content increase of the slab can be recalculated for the current timestep. Therefore, the OLSTC calculations are taking place continuously (with a 1 min interval as this is the frequency of the thermocouple measurements), allowing for tracking the evolution of the slab's average temperature across the furnace length.

### 2.2. Calculation of Slab Oxide Scale

The combustion products found in an atmosphere of a reheat furnace such as  $\text{H}_2\text{O}$ ,  $\text{CO}_2$ ,  $\text{O}_2$ ,  $\text{N}_2$ , and the very high temperatures create an aggressive oxidizing environment, in which steel products react with the furnace gas atmosphere through the processes of:<sup>[28]</sup> 1) an initial adsorption of free oxygen, 2) a chemical reaction to form a surface oxide, 3) a growth of the oxide scale, and 4) a cavity/microcrack/porosity formation within the film. As a result of this process, an oxide scale layer composed of wüstite, magnetite, and hematite forms on the surface of a reheated steel product, as shown in **Figure 1**.

At temperatures higher than 600 °C, the percent compositions of wüstite, magnetite, and hematite are, respectively, about 95:4:1%.<sup>[29]</sup> The OLSTC's oxide growth model adopts the 95:4:1% ratio. Due to the extremely high temperature in reheat furnaces, the rate of the oxide scale growth follows a parabolic regime<sup>[8]</sup> expressed by Equation (3)

$$M^2 = k_p t \text{ or } M = \sqrt{k_p t} \quad (3)$$

where  $M$  is mass of oxygen per unit area in  $\text{kg m}^{-2}$ , and  $k_p$  is the parabolic rate constant in  $\text{kg}^2 \text{m}^{-4} \text{s}^{-1}$ . The parabolic rate



**Figure 1.** Schematic representation of the typical oxide scale layer that forms as part of a steel reheating process.

constant is exponentially dependent on slab surface temperature, and it is given by Equation (4)

$$k_p = k_{p0} \cdot \exp(-E_a/RT_s) \quad (4)$$

where  $R$  is the universal gas constant ( $8.314 \text{ J mol}^{-1} \text{ K}^{-1}$ ),  $E_a$  is the activation energy in  $\text{J mol}^{-1}$ , and  $k_p$  is the parabolic oxidation rate coefficient in  $\text{kg}^2 \text{ m}^{-4} \text{ s}^{-1}$ . As stated in Section 2.1,  $T_s$  is the slab's surface temperature, which is calculated at 1-minute intervals meaning that  $M$  is also calculated on continuous basis with the same frequency. Therefore, each time the  $T_s$  is determined,  $M$  is also calculated. To convert between the calculated mass of oxygen per unit area,  $M$ , and the actual scale thickness,  $d$ , a conversion factor,  $C$  ( $\text{m}^3 \text{ kg}^{-1}$ ), is used, as shown in Equation (5)

$$d = M \cdot C + d_i, \quad \text{where } C = \frac{X}{(1 - \phi_{\text{scale}}) \cdot \rho_{\text{scale}}} \quad (5)$$

where  $d_i$  is the thickness of the oxide scale found on a slab prior to reheating,  $\rho_{\text{scale}}$  is the density of the scale ( $\text{kg m}^{-3}$ ),  $\phi_{\text{scale}}$  is the porosity of the formed oxide scale, which is a dimensionless quantity, and  $X$  is defined as per Equation (6)

$$X = \left( \frac{F_{\text{wustite}}}{Ox_{\text{wustite}}} + \frac{F_{\text{magnetite}}}{Ox_{\text{magnetite}}} + \frac{F_{\text{hematite}}}{Ox_{\text{hematite}}} \right)^{-1} \quad (6)$$

where  $Ox_{\text{phase}}$  is the mass of a given phase formed by oxidation in 1 kg oxygen and  $F_{\text{phase}}$  is the mass fraction of a given phase. Both  $Ox_{\text{phase}}$  and  $F_{\text{phase}}$  are experimentally determined quantities, where  $F_{\text{phase}}$  is the product of volume fraction of the phase and the density ratio of the given phase to scale,  $f_{\text{phase}} \cdot (\rho_{\text{phase}}/\rho_{\text{scale}})$ .

Having calculated the oxide scale thickness,  $d$ , and assuming constant values for the oxide scale's specific heat capacity,  $C_p$ , and the thermal conductivity,  $k$ , the Fourier's law of heat conduction (see Equation (2)) can be applied to calculate the heat conduction through the oxide scale layer, which will affect the heating of the slab. The thermal properties of the oxide scale are obtained from the model by Torres et al.<sup>[30]</sup>

### 3. Nondeterministic Approach to Uncertainty Quantification

Once the uncertainties are identified, they are approximated as PDFs and must be propagated through the underlying simulation model to quantify the output variability in the identified QoIs. The well-established MC method is the most straightforward and the

most robust technique to draw the random samples for propagation from the PDF-approximated uncertainties. However, the main drawback is that the MC procedure requires many system evaluations to yield reliable statistics as it relies on the law of large numbers, making it prohibitive for complex simulations such as OLSTC. Note, although OLSTC is a relatively time-consuming simulation, it is implemented online at Tata Steel facilities as a control mechanism thanks to significant computing resources, which are not available when the model is taken offline for analysis, like in the case of this work. Therefore, to overcome this limitation, the computationally expensive offline OLSTC model is replaced with a suitable statistical emulator also known as a surrogate model. A surrogate model is constructed based on approximating the response of the underlying simulator (OLSTC) to a limited number of strategically selected data points that need propagation through the simulator.

#### 3.1. Uncertainty Propagation and Sensitivity Analysis

It is prohibitive to perform statistical analyses, including sensitivity analyses (SA) over computationally expensive models such as the OLSTC. To overcome this, we create a surrogate model of the underlying simulator based on the PCE technique.<sup>[13,31]</sup> PCE approximates output of a model subject to uncertain inputs approximated as a vector of PDFs,  $\omega = (\omega_1, \dots, \omega_n) \in \Omega$  at a time,  $t$ , as an expansion in terms of polynomials, in the following form

$$f(\omega, t) \approx \sum_{k=0}^{N-1} \hat{f}_k \Psi_k(\omega, t) \quad (7)$$

where  $\Psi_k$  are orthogonal polynomials with respect to  $\omega$ ,  $\hat{f}_k$  is the expansion coefficient, and  $N$  is the cardinality dependent on the number of uncertain input and the degree of  $\Psi_k$ . The type of  $\Psi_k$  is selected based on the Wiener–Askey scheme.<sup>[32]</sup> Next, the goal is to calculate  $\hat{f}_k$ , which in our case is done nonintrusively by rearranging the above series for  $\hat{f}_k$  by exploiting the orthonormality of underlying basis<sup>[33]</sup>

$$\hat{f}_k = \frac{\langle f(\omega, t) \Psi_k \rangle}{\langle \Psi_k^2 \rangle} \quad \text{where } \langle f(\omega, t) \Psi_k \rangle \equiv \int_{\Omega} \Psi_k \rho(\omega, t) f(\omega, t) d\omega \quad (8)$$

and  $\rho$  is the density of  $\omega$  over  $\Omega$ .<sup>[10]</sup> For a given expansion (i.e., surrogate model),  $f(\omega, t)$ , the corresponding mean  $\mathbb{E}$ , and the variance  $\mathbb{V}$  of  $f(\omega, t)$  can be computed directly as a function of the PCE expansion coefficients

$$\mathbb{E}[f(t, \omega)] = \hat{f}_0 \quad \text{and} \quad \mathbb{V}[f(t, \omega)] = \sum_{k=1}^{N-1} \hat{f}_k^2 \quad (9)$$

Having calculated the model output variance,  $\mathbb{V}$ , it can be decomposed into contributions from the individual input parameters and their interactions using the Sobol' variance decomposition method,<sup>[34]</sup> sometimes referred to as functional ANOVA decomposition. Using the property that the ANOVA expansion is unique<sup>[34]</sup> and taking into account the orthonormal property of the basis,<sup>[33]</sup> the local Sobol' indices ( $S_i$ ), which measure individual contributions OR interactions between inputs and total

Sobol' indices ( $S_i^T$ ), which measure individual contributions and interactions between inputs (i.e.,  $\omega_i$  with  $\omega \neq i$ ) can be calculated as follows.

$$S_i(t) = \frac{\mathbb{V}[\mathbb{E}[f(\omega, t) | \omega_i]]}{\mathbb{V}[f(\omega, t)]}, \quad S_i^T(t) = \frac{\mathbb{V}[f(\omega, t) | \omega_{\sim i}]}{\mathbb{V}[f(\omega, t)]} \quad (10)$$

As part of this work, we focus on the total total-effect index.  $S_i^T(t)$  as parameter interaction in the complex system investigated is prevalent.

#### 4. Test Case and UQ Problem Statement

The methods above are applied to the OLSTC model of a top&bottom-fired walking beam reheat furnace of the hot strip mill (HSM) located in Tata Steel's Port Talbot steelworks. The reheating furnace features six zones, vestibule, recuperating, preheating, two heating zones, and a soaking zone. The function of this furnace is to raise the temperature of slabs to around 1250 °C using a mixture of coke oven and natural gases. The hot combustion products are ventilated toward the furnace's charging end to enable waste heat recuperation.

The data made available as part of this study was the thermocouple data (i.e., time-stamped  $T_f$  values, see Section 2.1) obtained for a 24 hr reheating period in November 2019, corresponding to the reheating of 83 carbon steel slabs. At Port Talbot's HSM, slabs of several different steel grades are reheated daily, some of which can be hot or cold charged. Within the OLSTC, steel grade differentiation is done via the input of the grade's temperature-dependent thermophysical properties. The target discharge temperature also varies over a wide range depending on the steel grade and the thickness of the slabs being rolled. The residence time will also vary based on different

factors such as the slab charging temperature and the slab thickness. Therefore, each reheating operation for an individual slab is expected to significantly vary from slab to slab. Based on this, it was deemed to be beneficial to perform subsequent analyses on the full day worth of reheating data and not base the analyses on an individual slab.

The variability in the OLSTC-modeled reheating behavior from slab to slab can be seen in **Figure 2**, which shows the slab temperature evolution and the oxide scale growth alongside their averages and zonal separation. Thus, to add robustness to the study, instead of looking at one individual slab, the forthcoming analyses will be performed for all 83 slabs with final results averaged to get a more realistic view of the intricacies of an actual reheating operation.

Note that the sudden drops in the average scale thickness seen in Figure 2 are the result of averaging. Specifically, this is partially caused because a number of slabs get discharged significantly quicker (i.e., hot-charged slabs need to spend less time undergoing reheating and will oxidize much earlier). The individual scale growth curves, as expected, are smooth.

##### 4.1. Characterization of Uncertain Input Space

As discussed in Section 2.1, the OLSTC model is primarily based on the measured thermocouple temperature data supplied at 1-minute intervals to construct a radiation curve (i.e.,  $T_f$  distribution across the furnace length) needed to calculate the slab's temperature evolution. Alongside the thermocouple data and the steel's thermophysical properties, the OLSTC model needs to know the slab's emissivity  $\epsilon_{\text{slab}}$ , the furnace free oxygen content  $O_2$  (%), the initial scale thickness  $d_i$  ( $\mu\text{m}$ ), and the scale porosity  $\varphi_{\text{scale}}$  (%), which are all treated as constants. Since the thermocouple temperature data and grade's thermophysical properties

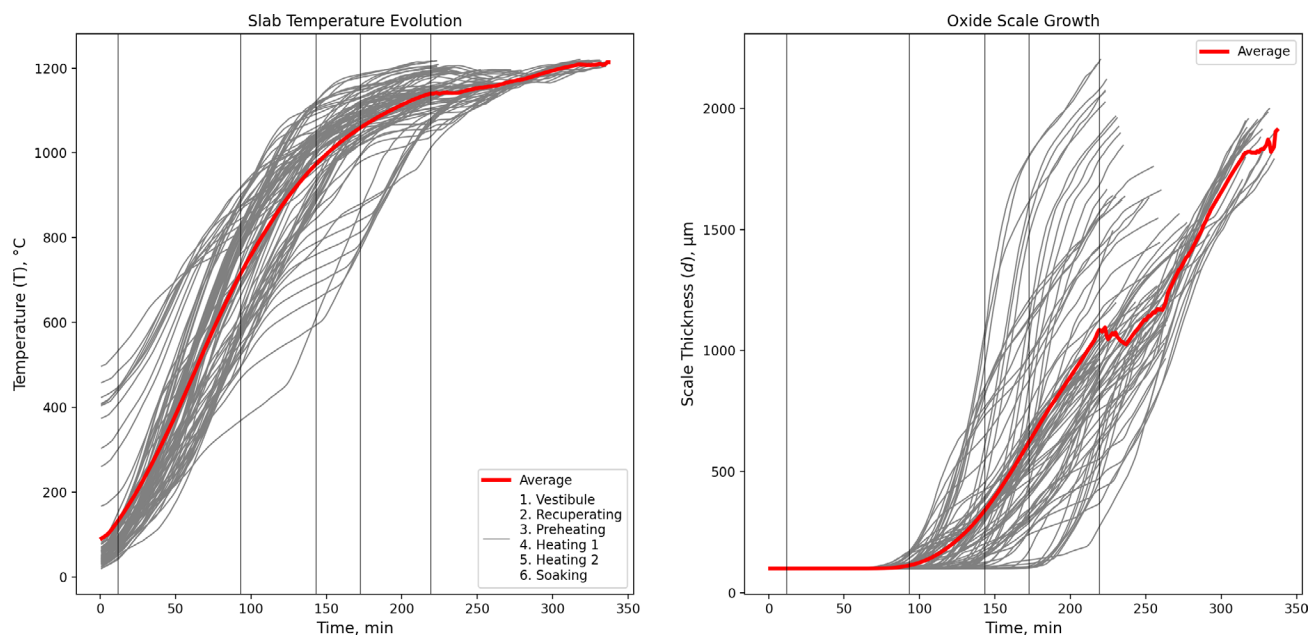


**Figure 2.** Individual and average slab temperature evolution and oxide scale growth of 83 slabs, reheated in a top and bottom-fired walking beam reheat furnace.

are measured, we treat those as part of the inner model workings rather than operational parameters that can vary and cause variability in the system.

More often than not, combustion, which determines the atmospheric furnace composition and dictates the growth of the oxide scale, in a reheating furnace is approached like a “black box”,<sup>[35]</sup> partially due to the difficulty and expenditure associated with performing experimental measurements in reheat furnace like conditions.<sup>[11]</sup> This suggests that the four remaining OLSTC inputs associated with the slab’s surface and atmospheric furnace composition are indeed uncertain and should be treated as probabilistic rather than deterministic (constant) to improve the model toward better physical representation. Every time a constant value is specified for any of these inputs (apart from  $d_i$  as that can be measured but that is rarely done), a large degree of assumption regarding a reheating operation is made.

Based on this, the four remaining OLSTC inputs,  $\epsilon_{\text{slab}}$ ,  $O_2$  (%),  $\varphi_{\text{scale}}$  (%), and  $d_i$  ( $\mu\text{m}$ ), are used to construct the PCE surrogate model aimed at approximating the slab temperature evolution and the oxide scale growth, which are the study’s QoIs, at the available data points (1 min interval). The PCE surrogate model is constructed over a probability space based on uncertain inputs that vary within specified bounds. Therefore, a surrogate model is only valid for predicting QoIs when supplied with inputs within the ranges used to construct the PCE surrogate. The uncertain input space,  $\Omega_r$ , is constructed based on the interval-valued OLSTC input parameters with the corresponding minimum and maximum values obtained based on literature findings as summarized in **Table 1**.

Note that unlike for all other parameters given in Table 1, the OLSTC model does not feature a direct input for free  $O_2$  content and instead deals with the parameter by linearly interpolating between the pre-exponential  $k_{p0}$  and the activation energy  $E_a$  constants used to solve for parabolic rate law (refer to Equation (4)) based on the concentration of that free  $O_2$  content in the furnace atmosphere. A fundamental assumption made with this approach, which is in line with literature findings,<sup>[36]</sup> is that the  $k_{p0}$  and  $E_a$  values are said to be linearly dependent on furnace free  $O_2$  content. Thus, by saying that free  $O_2$  content varies, what is in fact varied are the values of  $k_{p0}$ ,  $E_a$ . Note that the concentration of free oxygen content during a reheating process can vary between 1% and 5%.<sup>[8,37]</sup> For the furnace analyzed as part of this study, the values of the free  $O_2$  content have been reported to be between 1% and 2%; the values of  $k_p$  and  $E_a$  for this range are given in **Table 2** and were obtained via a gravimetric oxidation analysis of carbon steels in reheat atmospheres like conditions. This analysis was carried out at Tata Steel’s specialized oxidation laboratories.<sup>[38]</sup>

**Table 1.** Selected bounds of the uncertain OLSTC inputs.

Bounds/Uncertainty	$\epsilon_{\text{slab}}$ <sup>[44]</sup>	$O_2$ [%] <sup>[8,37]</sup>	$\varphi_{\text{scale}}$ [%] <sup>[45]</sup>	$d_i$ [ $\mu\text{m}$ ] <sup>[46]</sup>
Lower Bound	0.5	1	20	100
Upper Bound	0.9	2	45	500

## 5. Implementation and Results

### 5.1. Surrogate Modeling: PCE Surrogate Construction and Validation

For the propagation of input uncertainties, which are assumed to be uniformly distributed, a PCE approximation of the OLSTC model is constructed over the uncertain input parameter space  $\Omega_r$ .

$$\Omega_r \begin{cases} \omega_{\text{Slab}} & \sim \mathcal{U}(0.5, 0.9) \\ \omega_{O_2} & \sim \mathcal{U}(1, 2) \\ \omega_{\varphi_{\text{scale}}} & \sim \mathcal{U}(20, 45) \\ \omega_{d_i} & \sim \mathcal{U}(100, 500) \end{cases} \quad (11)$$

Chaospy 3.8,<sup>[39]</sup> a numerical toolbox for performing UQ, is utilized for the construction and evaluation of PCE models. To create a PCE surrogate model, a structure for the multivariate orthogonal polynomials,  $\Psi_k$ , corresponding to the joint PDF needs to be computed, which is done using the widely used three-term recurrence relation. As  $\Psi_k$  is linked to  $f(\omega, t)$  (refer to Equation (9)), the choice of the orthogonal basis depends on the PDF associated with the uncertain inputs. Since all the uncertain inputs are said to be uniformly distributed over  $\Omega_r$ , the uniform transformation  $\omega_i \sim \mathcal{U}(0, 1)$  corresponding to Legendre polynomials for  $\Psi_k$  is applied.

Here, PCE is based on multidimensional numerical integration based on the normal tensor product grid<sup>[40]</sup> combined with the classical Gaussian quadrature scheme that can be applied to any probability distribution.<sup>[41]</sup> For example, a Level-2 PCE expansion (PCE LVL 2), which means the second-order level of Gaussian quadrature of the 4D input space, requires 16 quadrature points, increasing to 81 points for a Level-3 PCE expansion (PCE LVL 3). Note to solve the integral given in Equation (8), in order to obtain the PCE surrogate, the underlying OLSTC simulator needs to be evaluated at all the generated quadrature points; thus, this is where the main computational effort occurs when applying the PCE framework.

In the Chaospy-based implementation depicted in **Figure 3**, the main inputs for generating the Gaussian quadrature, denoted by  $G$ , correspond to the PDFs of the four uncertain inputs (refer to Equation 11). The Gaussian quadrature order, selected as the third order ( $K = 3$ ), constitutes the only additional input. Because Python uses the index zero for the first entry of a list, ( $K-1$ ) has to be written in the code to account for the correct quadrature order  $K$ . Upon generating the 81 quadrature points ( $K^4$ ), we propagate the combinations of inputs through the OLSTC simulator in a black box manner. To construct the PCE surrogate,  $f(\omega, t)$ , and calculate the expansion coefficients,  $\hat{f}_k$ , we provide the generated nodes, weights (last row of table of Figure 3), model evaluations at these nodes, and the orthogonal polynomial expansion with the order of  $N = K = 3$ —obtained using Stieltjes’ recurrence algorithm

**Table 2.** Values of activation energy,  $E_a$ , and pre-exponential constant,  $k_{p0}$ , at 1% and 2% oxygen concentrations.<sup>[38]</sup>

Constants/ $O_2$ Concentration in %	1%	2%
$E_a$ [J mol <sup>-1</sup> ]	280 458	235 083
$k_{p0}$ , [kg <sup>2</sup> m <sup>-4</sup> s <sup>-1</sup> ]	1 384 530	33 695

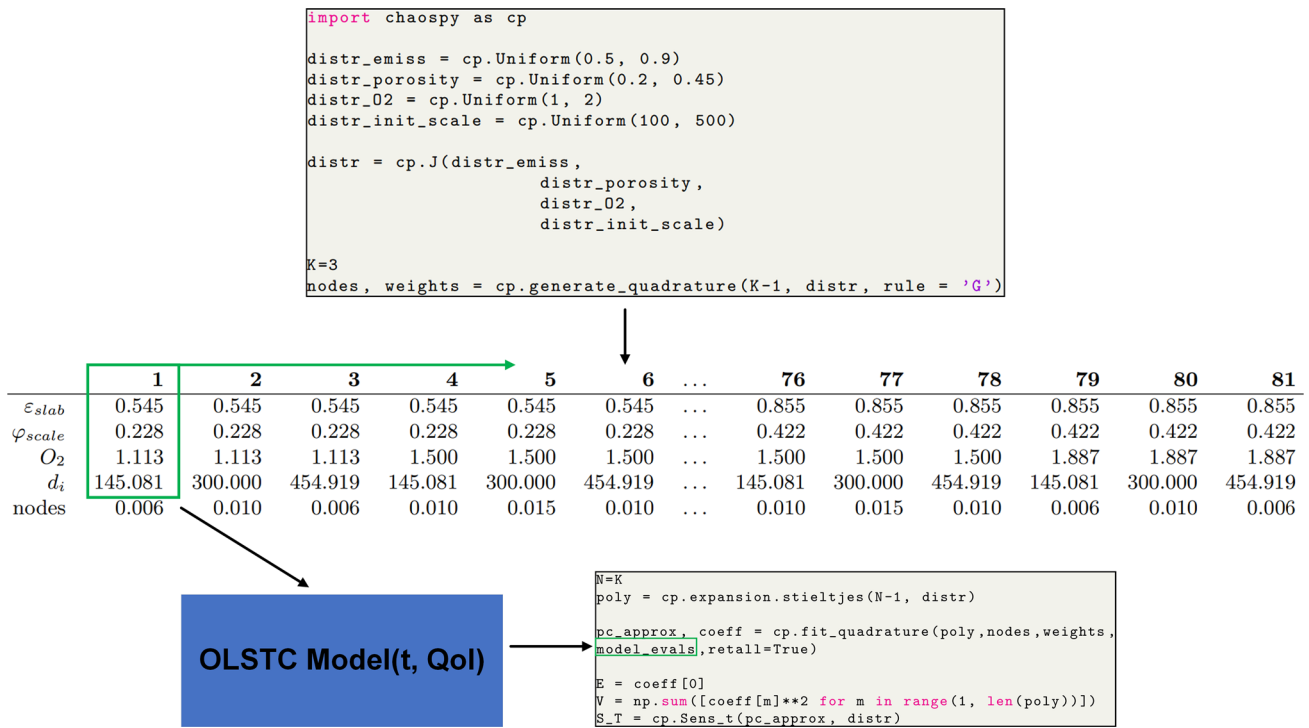


**Figure 3.** Chasopy-driven workflow for the propagation of the input uncertainties, the construction of a surrogate, and the estimation of the model's output statistics based on the PCE method.

method<sup>[42]</sup> to Chaospy's *fit\_quadrature* function. With the PCE surrogate and expansion coefficients in hand, we can compute output statistics, such as the mean,  $\mathbb{E}[f(t, \omega)]$ , and variance of the model output,  $\mathbb{V}[f(t, \omega)]$ , as well as the total effect Sobol indices  $S_i^T(t)$  for a given time (see Equation (9) and (10)). We must remind ourselves that the PCE surrogate has been constructed for all available 1-minute time stamps, with the most prolonged reheating duration being 336 min. This comprehensive approach, applied to 83 slabs, enables a truly representative statistical analysis of a steel reheating operation. However, significant computational resources and parallelization were necessary to accomplish this task.

PCE surrogate accuracy is examined through a qualitative comparison of the 83 slab-averaged temperature evolution and oxide scale growth from the OLSTC simulation and PCE with the expansion order of 3 (PCE LVL 3) at the deterministic input settings given as

$$\begin{cases} \varepsilon_{slab} &= 0.6 \\ O_2 &= 1\% \\ \varphi_{scale} &= 20\% \\ d_i &= 100 \mu\text{m} \end{cases} \quad (12)$$

The comparison is given in **Figure 4**, from which it is evident that PCE LVL three-surrogate model can accurately predict the in-question data at manageable computational costs ( $\approx 100$  hrs of CPU time). This implies we have obtained surrogate models at given times,  $t$  capable of mimicking the input/output behavior of the OLSTC simulator using polynomials allowing for cheap and accurate statistical analyses.

## 5.2. Zone-Based Overview of the PCE Surrogates and the Output Statistics

Examining the constructed surrogates in greater detail is helpful for a more comprehensive understanding of the process dynamics. To this end, **Table 3** provides a mathematical summary of the PCE-based UQ and SA, showcasing the actual polynomial used to approximate a given QoI,  $f(t, \omega)$ , along with the corresponding expansion coefficients,  $\hat{f}_k$ , the output variability associated with input uncertainties as quantified by  $\mathbb{E}[f(t, \omega)] \pm \sqrt{\mathbb{V}[f(t, \omega)]}$ , and the percentage contributions of these uncertainties and their interactions to the output variability quantified by  $S_i^T(t)$ . The selected reheating times correspond to the slab position in the middle of a given furnace zone based on the data from 83 slabs. This approach aims to provide readers with process insights at times of interest to reheat furnace practitioners, as all reheating furnaces consist of the same fundamental zones. While these zones may vary in length and other characteristics, their operating principles and main objectives remain consistent across all reheating furnaces, making the following reheating process insights generalizable.

## 5.3. Sensitivity Structure

To visualize the variability in slab temperature and oxide scale growth caused by the introduced input uncertainties, a plot of the QoI's PCE-derived standard deviation with a 95% confidence interval alongside the deterministic QoI is given in the top row of **Figure 5**. The standard deviation is simply derived from the

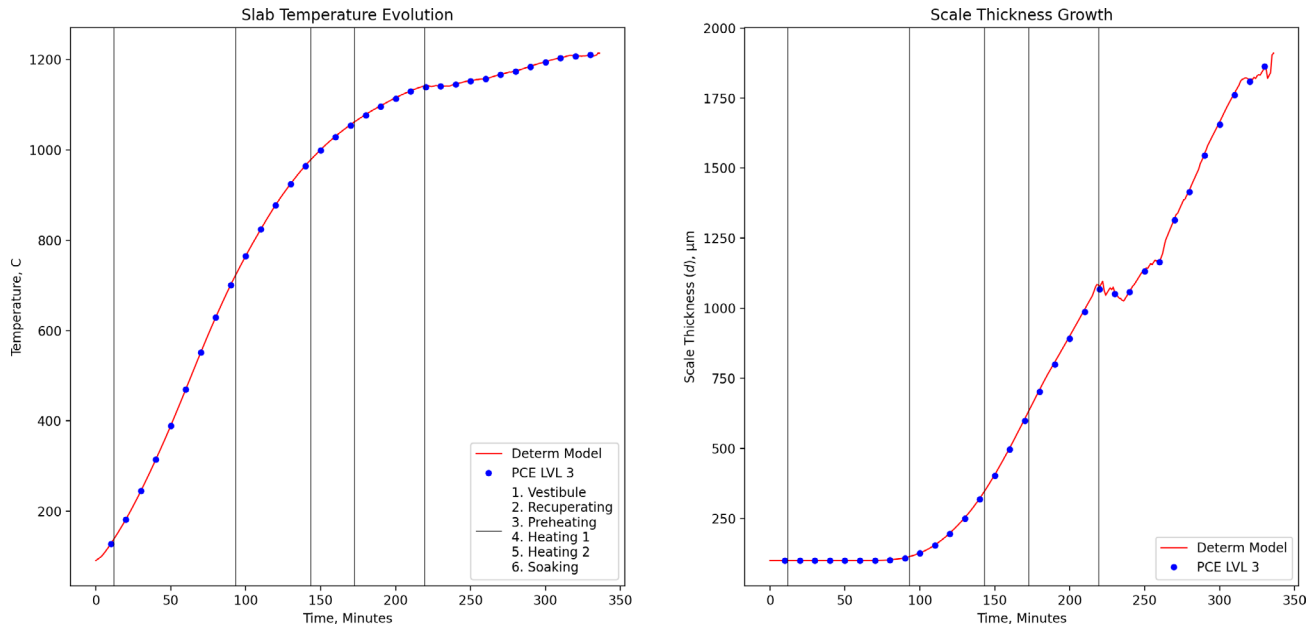


**Figure 4.** Comparison of slab temperature and oxide growth profiles from OLSTC simulation and PCE prediction.

PCE-based variance,  $\mathbb{V}$ , obtained as shown in Equation (8)–(11). The results indicate that the propagated uncertainties are exerting much more influence on the oxide scale growth than on the slab temperature. The standard deviation range quantifies this—the larger the range, the more variability in the system output is caused by the propagated uncertainties. Having obtained the output variability of both QoIs, total Sobol’ indices,  $S_i^T$ , can be obtained to reveal the individual contribution of the propagated uncertainties on the output QoI variability. Total Sobol indices,  $S_i^T$ , of the four propagated uncertainties for temperature evolution and oxide scale growth at 1 min intervals are shown in the Figure 5, bottom row.

Figure 5 shows that for the first  $\approx 100$  min of reheating, virtually all of the output variance in slab temperature is caused by the slab surface emissivity,  $\epsilon_{\text{slab}}$ . However, once the slabs enter the preheating zone, the dominance of  $\epsilon_{\text{slab}}$  starts to diminish and the influence exerted by the free  $\text{O}_2$  content and  $\varphi_{\text{scale}}$  parameters quickly starts to grow with free  $\text{O}_2$  content becoming the dominant parameter at around 270 min midway through the soaking zone. Scale porosity,  $\varphi_{\text{scale}}$ , also continually exerts more influence but is less influential than the free  $\text{O}_2$  content throughout the entire reheating operation and achieves an  $S_i^T$  of 0.2 toward the end of the soaking zone, which means that  $\varphi_{\text{scale}}$  influence on the slab’s discharge temperature is similar to the influence exerted by  $\epsilon_{\text{slab}}$ .

When it comes to the oxide scale growth, all of the output variance in the vestibule and majority of the preheating zone, up until the  $\approx 80$ th minute is caused by the initial scale thickness,  $d_i$ . However, once the slabs approach the preheating zone, the dominance of  $d_i$  rapidly decreases to a level where it exerts no influence on the QoI. At the time, when influence of  $d_i$  starts to rapidly go down, the influence of the three remaining parameters free  $\text{O}_2$  content,  $\varphi_{\text{scale}}$ , and  $\epsilon_{\text{slab}}$  start to quickly grow, with free  $\text{O}_2$  content and  $\varphi_{\text{scale}}$  becoming the most influential

parameters, causing about 60% and 20% of the discharge output variance respectively. The emissivity of the slab surface,  $\epsilon_{\text{slab}}$ , only shows significant influence ( $S_i^T \approx 0.5$ ) for a brief amount of time in the preheating zone and then becomes less influential as the slabs travel toward the soaking zone.

In summary, for both QoIs, free  $\text{O}_2$  content is the most influential parameter when it comes to the slab discharge, which makes it one of the most important parameters as the discharge slab characteristics are of utmost importance.<sup>[43]</sup> Free  $\text{O}_2$  content becomes the dominant parameter quicker in the case of the oxide scale growth. Scale porosity follows a similar but subdued trend as the free  $\text{O}_2$  content parameter for both QoIs. For both QoIs, the influence of  $\epsilon_{\text{slab}}$  continually decreases as the slabs travel toward the discharging end, with  $\epsilon_{\text{slab}}$  retaining slightly more influence in the case of slab temperature. Initial scale thickness,  $d_i$ , is completely unimportant to the slab’s temperature; however, it is the dominant parameter at the beginning of reheating in the case of the oxide scale growth.

## 6. Discussion

### 6.1. Quantity of Interest: Slab Temperature

During the start of reheating, the slab’s surface emissivity,  $\epsilon_{\text{slab}}$ , is critical to the heating of the slabs as the difference between the in-furnace radiation temperature,  $T_f$ , and slab’s surface temperature,  $T_s$ , is extremely large (refer to Equation (2)). This is reflected in the Sobol analysis depicted in the bottom row of Figure 5, showing that  $\epsilon_{\text{slab}}$  is the dominant parameter with respect to the slab temperature for a substantial segment of a reheating operation. However, the slab and furnace temperatures are nearly identical toward the discharge, with the heat transfer being reduced to a minimum, meaning that  $\epsilon_{\text{slab}}$  has a much

**Table 3.** Summary of the PCE-based UQ and SA at the times of interest, showing the polynomial approximation ( $T$ ,  $d$ ), the expansion coefficients  $f_k$ , confidence interval  $\mathbb{E}[f(t, \omega)] \pm \sqrt{\mathbb{V}[f(t, \omega)]}$ , and Sobol indices  $S_i^T(t)$ .

Reheating time/Slab's Qol	Temperature ( $T$ ), °C	Oxide scale thickness ( $d$ ), $\mu\text{m}$
Recup. Zone ( $t = 52$ mins.)	$T(t, \omega) = -0.04\epsilon_{\text{slab}}d_i - 0.016\varphi_{\text{scale}}\text{O}_2 - 0.044\epsilon_{\text{slab}}\text{O}_2 - 0.019\varphi_{\text{scale}} - 0.072\epsilon_{\text{slab}}\varphi_{\text{scale}} - 218.256\epsilon_{\text{slab}}^2 + 0.017d_i + 0.025\text{O}_2 + 0.072\varphi_{\text{scale}} + 672.015\epsilon_{\text{slab}} + 81.627$	$d(t, \omega) = -0.002\text{O}_2d_i - 0.003\varphi_{\text{scale}}d_i - 0.007\epsilon_{\text{slab}}d_i - 0.106\text{O}_2^2 + 2.247\varphi_{\text{scale}}\text{O}_2 + 5.073\epsilon_{\text{slab}}\text{O}_2 + 2.724\varphi_{\text{scale}}^2 + 8.615\epsilon_{\text{slab}}\varphi_{\text{scale}} + 8.796\epsilon_{\text{slab}}^2 + 1.005d_i - 2.677\text{O}_2 - 9.122\varphi_{\text{scale}} - 17.753\epsilon_{\text{slab}} + 7.511$
	$\hat{f}_k = [438.543, -1.428, -0.002, -0.001, 40.904, -0.013, 0, 0, 0, 0, -0.539, -0.001, -0.001, -2.603]$	$\hat{f}_k = [300.427, 115.361, 0.222, 0.091, 0.341, 0.04, -0.057, -0.008, -0.022, 0.047, 0.013, -0.09, 0.169, 0.072, 0.105]$
	$\mathbb{E}[T(t, \omega)] \pm \sqrt{\mathbb{V}[T(t, \omega)]} = 438.543^\circ\text{C} \pm 41.04$	$\mathbb{E}[d(t, \omega)] \pm \sqrt{\mathbb{V}[d(t, \omega)]} = 300.427\mu\text{m} \pm 115.37$
	$S_i^T(t): \epsilon_{\text{slab}} = 99.719\%, \varphi_{\text{scale}} = 0.005\%, \text{O}_2 = 0.005\%, d_i = 0.264\%$	$S_i^T(t): \epsilon_{\text{slab}} = 0.032\%, \varphi_{\text{scale}} = 0.041\%, \text{O}_2 = 0.039\%, d_i = 99.983\%$
Preheating Zone ( $t = 118$ mins.)	$T(t, \omega) = 0.008\text{O}_2d_i + 0.014\varphi_{\text{scale}}d_i - 0.063\epsilon_{\text{slab}}d_i + 9.889\text{O}_2^2 - 15.43\varphi_{\text{scale}}\text{O}_2 - 33.632\epsilon_{\text{slab}}\text{O}_2 - 28.266\varphi_{\text{scale}}^2 - 77.051\epsilon_{\text{slab}}\varphi_{\text{scale}} - 543.146\epsilon_{\text{slab}}^2 - 0.022d_i - 11.114\text{O}_2 + 74.685\varphi_{\text{scale}} + 1233.409\epsilon_{\text{slab}} + 348.448$	$d(t, \omega) = -0.206\text{O}_2d_i - 0.41\varphi_{\text{scale}}d_i - 1.084\epsilon_{\text{slab}}d_i - 494.667\text{O}_2^2 + 698.386\varphi_{\text{scale}}\text{O}_2 + 1091.538\epsilon_{\text{slab}}\text{O}_2 + 1411.02\varphi_{\text{scale}}^2 + 2902.424\epsilon_{\text{slab}}\varphi_{\text{scale}} + 218.161\epsilon_{\text{slab}}^2 + 1.55d_i + 883.307\text{O}_2 - 3092.115\varphi_{\text{scale}} - 1146.577\epsilon_{\text{slab}} - 282.64$
	$\hat{f}_k = [889.252, -6.733, -2.204, -1.193, 43.706, -0.174, 0.263, 0.737, 0.118, 0.321, -0.132, -0.845, -1.121, -0.642, -6.477]$	$\hat{f}_k = [649.101, 71.503, 94.828, 56.387, 164.008, 5.367, -6.874, -36.87, -3.417, 14.55, 6.573, -14.449, 36.385, 24.187, 2.602]$
	$\mathbb{E}[T(t, \omega)] \pm \sqrt{\mathbb{V}[T(t, \omega)]} = 889.252^\circ\text{C} \pm 44.97$	$\mathbb{E}[d(t, \omega)] \pm \sqrt{\mathbb{V}[d(t, \omega)]} = 649.101\mu\text{m} \pm 242.74$
	$S_i^T(t): \epsilon_{\text{slab}} = 96.724\%, \varphi_{\text{scale}} = 0.204\%, \text{O}_2 = 0.568\%, d_i = 2.5\%$	$S_i^T(t): \epsilon_{\text{slab}} = 40.263\%, \varphi_{\text{scale}} = 4.486\%, \text{O}_2 = 15.291\%, d_i = 35.574\%$
Heating Zone ( $t = 177$ mins.)	$T(t, \omega) = 0.006\text{O}_2d_i + 0.01\varphi_{\text{scale}}d_i + 0.028\epsilon_{\text{slab}}d_i + 25.016\text{O}_2^2 - 26.619\varphi_{\text{scale}}\text{O}_2 - 22.467\epsilon_{\text{slab}}\text{O}_2 - 56.602\varphi_{\text{scale}}^2 - 61.573\epsilon_{\text{slab}}\varphi_{\text{scale}} - 397.741\epsilon_{\text{slab}}^2 - 0.055d_i - 68.189\text{O}_2 + 79.978\varphi_{\text{scale}} + 786.858\epsilon_{\text{slab}} + 802.103$	$d(t, \omega) = -0.208\text{O}_2d_i - 0.515\varphi_{\text{scale}}d_i - 0.588\epsilon_{\text{slab}}d_i - 1958.927\text{O}_2^2 + 1814.469\varphi_{\text{scale}}\text{O}_2 + 1378.331\epsilon_{\text{slab}}\text{O}_2 + 4447.637\varphi_{\text{scale}}^2 + 4293.053\epsilon_{\text{slab}}\varphi_{\text{scale}} - 3012.874\epsilon_{\text{slab}}^2 + 0.792d_i + 5403.409\text{O}_2 - 5751.003\varphi_{\text{scale}} + 3621.697\epsilon_{\text{slab}} - 4769.163$
	$\hat{f}_k = [1068.647, -4.203, -4.552, -2.656, 21.323, -0.254, 0.195, 1.865, 0.084, -0.555, -0.264, 0.371, -0.749, -0.513, -4.743]$	$\hat{f}_k = [1727.463, 16.117, 294.059, 195.747, 310.616, 4.757, -6.946, -146.01, -4.29, 37.801, 20.719, -7.84, 45.944, 35.775, -35.931]$
	$\mathbb{E}[T(t, \omega)] \pm \sqrt{\mathbb{V}[T(t, \omega)]} = 1068.647^\circ\text{C} \pm 23.43$	$\mathbb{E}[d(t, \omega)] \pm \sqrt{\mathbb{V}[d(t, \omega)]} = 1727.463\mu\text{m} \pm 507.67$
	$S_i^T(t): \epsilon_{\text{slab}} = 85.168\%, \varphi_{\text{scale}} = 2.493\%, \text{O}_2 = 8.273\%, d_i = 3.429\%$	$S_i^T(t): \epsilon_{\text{slab}} = 38.653\%, \varphi_{\text{scale}} = 13.351\%, \text{O}_2 = 39.908\%, d_i = 5.406\%$
Soaking Zone ( $t = 300$ mins.)	$T(t, \omega) = 0.001\text{O}_2d_i + 0.001\varphi_{\text{scale}}d_i + 0.014\epsilon_{\text{slab}}d_i + 36.862\text{O}_2^2 - 25.914\varphi_{\text{scale}}\text{O}_2 - 2.81\epsilon_{\text{slab}}\text{O}_2 - 66.974\varphi_{\text{scale}}^2 - 15.721\epsilon_{\text{slab}}\varphi_{\text{scale}} - 92.627\epsilon_{\text{slab}}^2 - 0.015d_i - 120.315\text{O}_2 + 43.908\varphi_{\text{scale}} + 170.092\epsilon_{\text{slab}} + 1215.268$	$d(t, \omega) = -0.104\text{O}_2d_i - 0.322\varphi_{\text{scale}}d_i + 0.02\epsilon_{\text{slab}}d_i - 4336.615\text{O}_2^2 + 3317.997\varphi_{\text{scale}}\text{O}_2 + 1087.854\epsilon_{\text{slab}}\text{O}_2 + 8970.91\varphi_{\text{scale}}^2 + 3715.434\epsilon_{\text{slab}}\varphi_{\text{scale}} - 3819.79\epsilon_{\text{slab}}^2 + 0.112d_i + 13235.729\text{O}_2 - 7576.718\varphi_{\text{scale}} + 5098.551\epsilon_{\text{slab}} - 9878.956$
	$\hat{f}_k = [1178.954, -1.035, -5.737, -3.549, 4.083, -0.11, 0.027, 2.747, 0.009, -0.54, -0.312, 0.19, -0.094, -0.131, -1.105]$	$\hat{f}_k = [3614.786, -4.871, 587.357, 413.928, 299.793, 1.814, -3.452, -323.232, -2.684, 6.125, 41.791, 0.273, 36.262, 30.962, -45.554]$
	$\mathbb{E}[T(t, \omega)] \pm \sqrt{\mathbb{V}[T(t, \omega)]} = 1178.954^\circ\text{C} \pm 8.63$	$\mathbb{E}[d(t, \omega)] \pm \sqrt{\mathbb{V}[d(t, \omega)]} = 3614.786\mu\text{m} \pm 850.58$
	$S_i^T(t): \epsilon_{\text{slab}} = 24.729\%, \varphi_{\text{scale}} = 17.492\%, \text{O}_2 = 55.923\%, d_i = 1.498\%$	$S_i^T(t): \epsilon_{\text{slab}} = 12.923\%, \varphi_{\text{scale}} = 24.037\%, \text{O}_2 = 62.278\%, d_i = 0.091\%$

less significant impact on how much heat gets into the slab and thereby,  $\epsilon_{\text{slab}}$  has less impact on the slab temperature distribution.

The oxide scale formed on the slab surface significantly affects the heat transfer characteristics of the slab because the thermal conductivity of the oxide scale is much smaller than that of steel. Therefore, the oxide scale reduces the radiative heat transfer from the hot furnace gases and the walls to the slab. As the oxide scale grows, the heat transport is reduced further. Thus, toward the discharge, when the slab's temperature equilibrated with the surroundings so that  $T_f \approx T_s$  (refer to Equation (2)) and a significant oxide scale layer has been formed, the heat absorbed by the formed oxide scale becomes substantial. This significantly affects the heating of the slabs, which implies that the free  $\text{O}_2$  content is now very influential as it is positively correlated with the growth of the oxide scale layer as per Equation (4).

Scale porosity,  $\varphi_{\text{scale}}$ , also becomes an important parameter toward the discharge as in the case with free  $\text{O}_2$  content because it is also positively correlated to the growth of the oxide scale (refer to Equation (5)). Still, scale porosity has less impact on slab heating than the thickness of the scale, whose formation is dominated mainly by the free  $\text{O}_2$  content.

The initial scale thickness plays an insignificant role in influencing the slab heating. This is because, at the start of reheating operation, when the initial scale thickness is expected to exert some influence, there is a significant difference between  $T_f$  and  $T_s$ , which means that the other propagated parameters are virtually negligible in comparison to the slab emissivity,  $\epsilon_{\text{slab}}$ . The influence of the initial scale thickness,  $d_i$ , fails to pick up even after  $T_f$  and  $T_s$  equilibrated by that point; the thickness of the formed oxide scale,  $d$ , is much larger than the initial scale thickness,  $d_i$  (refer to Equation (5)).



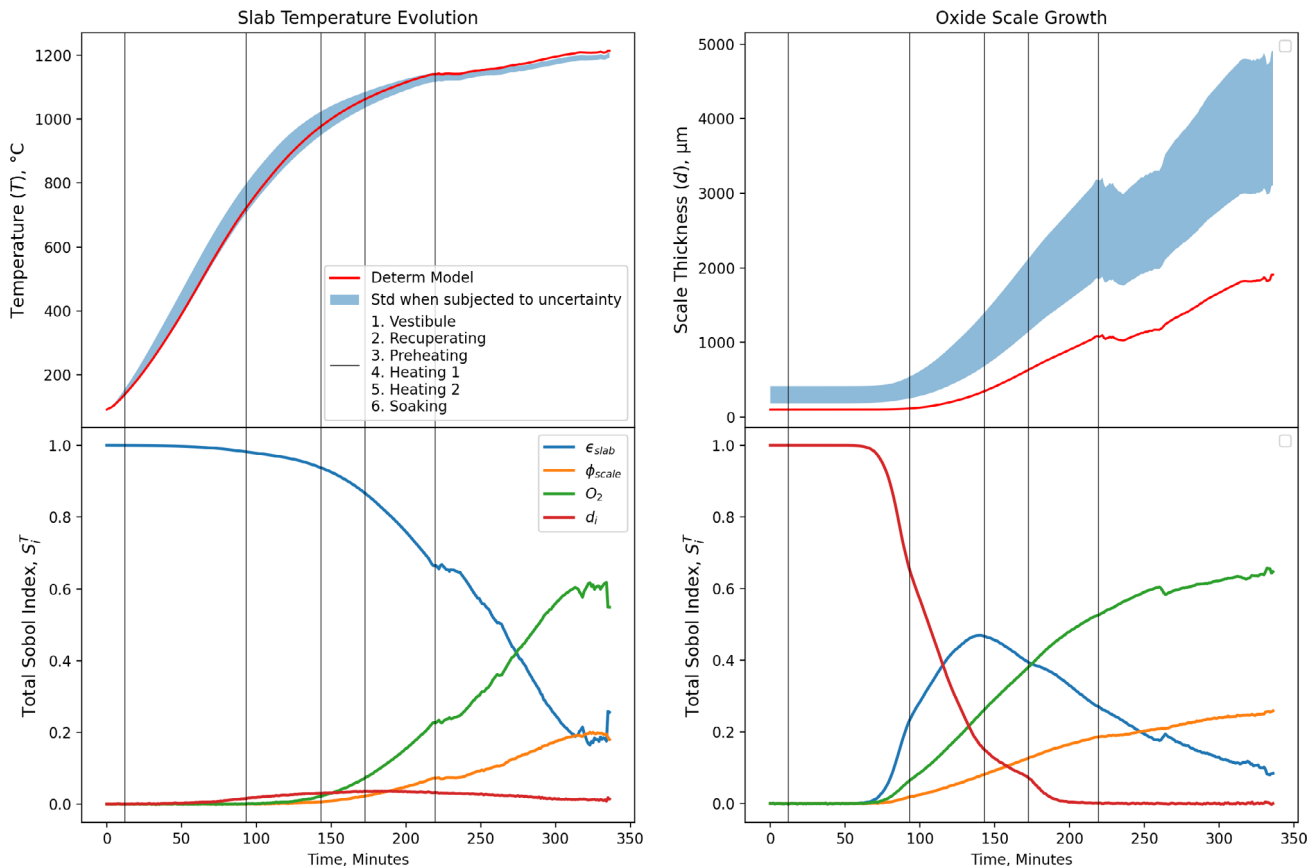


**Figure 5.** Total Sobol indices for slab temperature evolution and oxide scale growth.

As the oxide scale grows during reheating and so does its influence on the heating of the slabs, the parameters associated with the scale formation ( $O_2$ ,  $\varphi_{scale}$ ) are consequently the ones that continuously increase their influence on the temperature of the slabs as they travel through the furnace.

## 6.2. Quantity of Interest: Oxide Scale Thickness

During the beginning of reheating, scale formation is not taking place (refer Figure 2, which shows that the oxide scale only starts to form after  $\approx 100$  min of reheating). Therefore, during those 100 min, all of the output variance in scale thickness is attributed to the uncertainty in the initial scale thickness,  $d_i$ . To put it simply, before the formation of the oxide scale, its thickness is equal to  $d_i$ , suggesting that only  $d_i$  can possibly cause any output variability. However, the moment the slabs do start to scale, the impact of  $d_i$  rapidly disappears as the scale thickness associated with the in-furnace scale formation is much larger than that of the initial scale. As established, the in-furnace scale formation depends on free  $O_2$  content and scale porosity,  $\varphi_{scale}$ ; thus, they become the dominant parameters as soon as the oxide scale starts to grow, which in the case of the furnace analyzed occurs after  $\approx 100$  min of reheating (see Figure 4). However, shortly after the scale begins to form, there is an interval when the slab emissivity,  $\epsilon_{slab}$  is the dominant parameter concerning scale growth. As

established,  $\epsilon_{slab}$  strongly influences the resulting radiative heat flux impinging onto the slab surface,  $q$  (refer to Equation (2)), which dictates the surface temperature of that slab,  $T_s$ , a component in the calculation of the parabolic rate constant,  $k_{p0}$  as per Equation (4), which, in turn, dictates the rate of the scale growth. Thus, in that interval when  $q$  is still significant as  $T_f \gg T_s$ , the slab emissivity is a dominant parameter as it substantially impacts  $q$  and  $T_s$ . However, when the heat transfer between the slab and the surroundings slows, furnace-free  $O_2$  content and scale porosity,  $\varphi_{scale}$ , expectedly dominate as they are the parameters ultimately dictating the rate of the oxide scale growth. Therefore, the slab's emissivity becomes less critical to the growth of the oxide scale as the slabs move toward the discharge and reach the temperature of the surroundings.

## 7. Conclusion

The present study demonstrated a successful application of the nonintrusive PCE method for UQ in the simulation of slab reheating based on the OLSTC model by Tata Steel. The “offline” version of the OLSTC model made available as part of this study is computationally expensive, making direct sampling techniques for probabilistic UQ analysis (i.e., MC sampling) prohibitive. This required using surrogating techniques for forward propagation of uncertainties, which in our case was the PCE.

UQ of reheat furnace simulations is deemed an important area of research as these systems are highly complex, in which it is highly desirable to characterize the input parameter space often associated with uncertainty and the corresponding impact on computed results.

In reheat furnace simulations, a major source of uncertainty is introduced when specifying the surface properties of a slab and furnace atmospheric conditions, quantities that are very difficult to measure experimentally and are generally used as “tuning parameters” with basic physical restrictions applied, that is, the emissivity of a slab surface cannot be more than unity. Because it is not representative to treat slab surface and furnace atmospheric properties as deterministic, they were defined as uncertain and approximated as PDFs of uniform distribution with the respective bounds obtained based on literature findings. The impact of the defined input uncertainties was observed for the output QoIs of slab temperature evolution and the oxide scale growth. The constructed PCE surrogate models of both QoIs were validated against the deterministic reference OLSTC simulation.

Specifically, the inputs propagated as part of this study were the emissivity of the slab’s surface  $\epsilon_{\text{slab}}$ , the furnace free oxygen content,  $O_2(\%)$ , the initial scale thickness  $d_i(\mu\text{m})$ , and the scale porosity  $\varphi_{\text{scale}}$ . PCE surrogate models for each available timed data point were validated by comparing the 83 slab-averaged temperature evolution and oxide scale growth from the OLSTC simulation to the PCE surrogate model of third order at the deterministic input settings. The computationally inexpensive PCE surrogate models were used to obtain the probabilistic bounds of the study’s QoIs, represented in this study as the standard deviation with a 95% confidence interval. This analysis revealed a substantial uncertainty region in the oxide scale growth. The uncertainty region for slab temperature was significantly smaller, suggesting that the introduced uncertainties had a much more significant impact on the growth of the oxide scale.

Sobol SA revealed that for most of the reheating operation, the majority of the output variance in the slab temperature was linked to the emissivity of the slab surface,  $\epsilon_{\text{slab}}$ . However, the influence of  $\epsilon_{\text{slab}}$  was found to be continually declining as the slabs got hotter. Free  $O_2$  content and oxide scale porosity,  $\varphi_{\text{scale}}$  parameters exhibited opposite behavior, which saw free  $O_2$  content becoming the dominant parameter and  $\varphi_{\text{scale}}$  reaching the same level influence as  $\epsilon_{\text{slab}}$  about a midway through the soaking zone (see Figure 2).

These dynamics are observed, because, as the surface temperature of the slab and the in-furnace temperature equilibrate during the reheating, the influence associated with the emissivity of the slab continually declines, while at the same time, the oxide scale growth becomes significant, making it an increasingly influential parameter as the slabs travel toward the discharge end. Therefore, the parameters directly associated with the growth of the oxide scale become increasingly important, with free oxygen content becoming the most influential parameter concerning the discharge temperature of the slab.

When it comes to the QoI of the oxide scale growth, nearly all of the output variance was caused by the uncertainty in the initial scale thickness until the end of the recuperating zone. However, as soon as the oxide scale starts to grow, the impact of  $d_i$  rapidly disappears as the scale thickness associated with the in-furnace

scale formation is much larger than that of the initial scale. As established, the in-furnace scale formation predominantly depends on free  $O_2$  content and scale porosity,  $\varphi_{\text{scale}}$ ; thus, they become the dominant parameters as soon as the scale starts to grow, which in the case of the furnace analyzed occurs at the start of the preheating zone (see Figure 5).

## Acknowledgements

The authors thank Ben Martin, Imrul Kayes, Jonathon Richards from Tata Steel in the UK and Wanda Melfo Prada from Tata Steel in Europe for valuable discussions on the industrial context of this research.

## Conflict of Interest

The authors declare no conflict of interest.

## Data Availability Statement

The data that support the findings of this study are available from the corresponding author upon reasonable request.

## Keywords

polynomial chaos expansion, reheat furnaces, uncertainty quantification

Received: July 4, 2022

Revised: April 3, 2023

Published online:

- [1] K. D. Kantarakias, K. Shawki, G. Papadakis, *Phys. Rev. E*, **2020**, *101*, 022223.
- [2] N. Loshkarev, V. Noskov, G. Druyhinin, *KnE Eng.* **2018**, *3*, 287.
- [3] M.-J. Huang, C.-T. Hsieh, S.-T. Lee, C.-H. Wang, *Numer. Heat Transfer, Part A* **2008**, *54*, 625.
- [4] T. Morgado, P. J. Coelho, P. Talukdar, *Appl. Therm. Eng.* **2015**, *76*, 496.
- [5] J. G. Kim, K. Y. Huh, I. T. Kim, *Numer. Heat Transfer, Part A* **2000**, *38*, 589.
- [6] K. Lin, M. Pourmajidian, F. K. Suleiman, J. R. McDermid, K. J. Daun, *Metall. Mater. Trans. B* **2022**, *53*, 380.
- [7] C. H. Louise, *Emissivity and Oxidation Evolution in Reheating Furnace Environments*, Swansea University **2019**, <https://gtr.ukri.org/projects?ref=studentship-2610326>.
- [8] P. Wikström, Y. Weihong, W. Blasiak, *Steel Res. Int.* **2008**, *79*, 765.
- [9] G. Tang, B. Wu, D. Bai, Y. Wang, R. Bodnar, C. Zhou, *Appl. Therm. Eng.* **2018**, *132*, 779.
- [10] J. Prager, H. N. Najm, K. Sargsyan, C. Safta, W. J. Pitz, *Combust. Flame* **2013**, *160*, 1583.
- [11] B. J. Peter Mullinger, *Industrial and Process Furnaces: Principles, Design and Operation*, 2nd ed., Elsevier, Oxford, UK **2014**.
- [12] A. Forrester, A. Sobester, A. Keane, *Engineering Design Via Surrogate Modelling: A Practical Guide*, John Wiley & Sons, Ltd **2008**.
- [13] O. P. Le Maître, O. M. Knio, *Spectral Methods for Uncertainty Quantification: With Applications to Computational Fluid Dynamics*, Springer, Dordrecht **2010**.
- [14] T. Crestaux, O. Le Maître, J.-M. Martinez, *Reliab. Eng. Syst. Saf.* **2009**, *94*, 1161.

- [15] K. D. Kantarakias, K. Shawki, G. Papadakis, *Phys. Rev. E* **2020**, *101*, 022223.
- [16] K. Sepahvand, S. Marburg, H.-J. Hardtke, *Int. J. Appl. Mech.* **2010**, *2*, 305.
- [17] M. V. C. de Souza, M. J. Colaço, A. J. K. Leiroz, *Fuel* **2014**, *134*, 358.
- [18] F. S. Hover, M. S. Triantafyllou, *Automatica* **2006**, *42*, 789.
- [19] K. Sepahvand, S. Marburg, H.-J. Hardtke, *Int. J. Appl. Mech.* **2011**, *3*, 587.
- [20] P. Sumant, H. Wu, A. Cangellaris, N. Aluru, *IEEE Trans. Antennas Propag.* **2011**, *60*, 301.
- [21] H. N. Najm, *Annu. Rev. Fluid Mech.* **2009**, *41*, 35.
- [22] D. Staalman, B. Martin, R. Speets, P. Pronk, K. White, *Project Report - On-Line Slab Temperature Calculation and Control (OLSTC/C)*, Tata Steel Research **2015**, pp. 1–12, <https://doi.org/10.13140/RG.2.1.3129.7762>.
- [23] A. K. Dirk Staalman, in *Proc. IMECE96: Int. Mechanical Engineering Congress and Exposition*, Hoogovens Research & Development, Atlanta, GA, November **1996**.
- [24] D. Staalman, *Metall. Res. Technol.* **2004**, *101*, 453.
- [25] J. Harish, P. Dutta, *Ironmaking Steelmaking* **2005**, *32*, 151.
- [26] H. D. Baehr, K. Stephan, *Heat and Mass Transfer*, Springer-Verlag, Berlin **2011**.
- [27] I. Liu, *Continuum Mech. Thermodyn.* **1990**, *2*, 301.
- [28] M. Y. Kim, *Int. J. Mech. Mechatron. Eng.* **2013**, *7*, 1337.
- [29] J. Tominaga, K.-Y. Wakimoto, T. Mori, M. Murakami, T. Yoshimura, *Trans. Iron Steel Inst. Jpn.* **1982**, *22*, 646.
- [30] M. Torres, R. Colas, *J. Mater. Process. Technol.* **2000**, *105*, 258.
- [31] R. G. Ghanem, P. D. Spanos, *Stochastic Finite Elements: A Spectral Approach*, Springer, New York, NY **1991**, pp. 67–99.
- [32] D. Xiu, G. E. Karniadakis, *SIAM J. Sci. Comput.* **2002**, *24*, 619.
- [33] R. Koekoek, P. A. Lesky, R. F. Swarttouw, *Hypergeometric Orthogonal Polynomials and Their Q-Analogues*, 1st ed., Springer, Berlin **2010**.
- [34] I. M. Sobol, *Math. Comput. Simul.* **2001**, *55*, 271.
- [35] S. Gangoli, G. Buragino, X. He, E. Arslan, P. Verderame, R. Hendershot, A. Slavejko, F. Bellis, L. Bellis, J. McCarthy, R. Cross, *Importance of Control Strategy for Oxy-Fuel Burners in a Steel Reheat Furnace*, Air Products and Chemicals, Inc. **2013**.
- [36] H. Abuluwefa, R. Guthrie, F. Ajersch, *Oxid. Met.* **1996**, *46*, 423.
- [37] H.-H. Cheng, Y.-L. Hsu, C. Wang, F. Hsia, T.-T. Ou, *Tech. Rep.* **2011**, *24*, 20.
- [38] S. Faber, V. Hasselt, *Oxidatieonderzoek Met Behulp Van Thermobalans*, Tech. rep., Corporate Research Laboratorium Walserijprocessen en Metaalkunde, IJmuiden, Arch.lab, nr. 75246 **1992**.
- [39] J. Feinberg, H. Langtangen, *J. Comput. Sci.* **2015**, *11*, 46.
- [40] M. Eldred, J. Burkardt, in *47th AIAA Aerospace Sciences Meeting Including the New Horizons Forum and Aerospace Exposition*, Orlando, FL, January **2009**, p. 976.
- [41] P. J. Davis, P. Rabinowitz, in *Computer Science and Applied Mathematics*, Academic Press, New York, NY **1984**.
- [42] W. Gautschi, *SIAM J. Sci. Stat. Comput.* **1982**, *3*, 289.
- [43] G. Tang, B. Wu, D. Bai, Y. Wang, R. Bodnar, C. Q. Zhou, *Int. J. Heat Mass Transfer* **2017**, *113*, 1142.
- [44] G. W. Lee, M. Y. Kim, *Manuf. Eng.* **2014**, *8*, 922.
- [45] O. Resl, M. Chabicovsky, H. Votavová, in *Proc. Engineering Mechanics Conf. 2019*, Svratka, Czech Republic, May **2019**, pp. 315–318, <https://doi.org/10.21495/71-0-315>.
- [46] R. M. P. Huitron, P. E. R. López, E. Vuorinen, P. N. Jalali, L. Pelcastre, M. Kärkkäinen, *Metals* **2020**, *10*, 1243.